Analyses of combined Merkel cell carcinomas with neuroblastic components suggests that loss of T antigen expression in Merkel cell carcinoma may result in cell cycle arrest and neuroblastic transdifferentiation

Thibault Kervarrec, Silke Appenzeller, Susanne Gramlich, Etienne Coyaud, Kamel Bachiri, Romain Appay, Nicolas Macagno, Anne Tallet, Christine Bonenfant, Yannick Lecorre, et al.

Journal of Pathology
J Pathol September 2024; **264:** 112–124
Published online 25 July 2024 in Wiley Online Library
(wileyonlinelibrary.com) DOI: 10.1002/path.6304

ORIGINAL ARTICLE

Analyses of combined Merkel cell carcinomas with neuroblastic components suggests that loss of T antigen expression in Merkel cell carcinoma may result in cell cycle arrest and neuroblastic transdifferentiation

Thibault Kervarrec[1,2,3*], Silke Appenzeller[4], Susanne Gramlich[5], Etienne Coyaud[6], Kamel Bachiri[6], Romain Appay[7], Nicolas Macagno[3,7], Anne Tallet[8], Christine Bonenfant[8], Yannick Lecorre[9], Jean Kapfer[10], Sami Kettani[11], Nalini Srinivas[12], Kuan Cheok Lei[12,13], Anja Lange[14], Jürgen C Becker[12,13], Eva Maria Sarosi[15], Hervé Sartelet[16,17], Andreas von Deimling[18,19], Antoine Touzé[2], Serge Guyétant[1,2], Mahtab Samimi[2,3,20], David Schrama[15†] and Roland Houben[15†]

[1] *Department of Pathology, Université de Tours, Centre Hospitalier Universitaire de Tours, Tours, France*
[2] *"Biologie des infections à polyomavirus" team, UMR INRAE ISP 1282, Université de Tours, Tours, France*
[3] *CARADERM Network*
[4] *Comprehensive Cancer Center Mainfranken, University Hospital of Würzburg, Würzburg, Germany*
[5] *Institute of Pathology, University of Würzburg, Würzburg, Germany*
[6] *PRISM INSERM U1192, Université de Lille, Lille, France*
[7] *Department of Pathology, Université de Marseille, Assistance publique des Hopitaux de Marseille, Marseille, France*
[8] *Platform of Somatic Tumor Molecular Genetics, Centre Hospitalier Universitaire de Tours, Tours, France*
[9] *Dermatology Department, LUNAM Université, CHU Angers, Angers, France*
[10] *Cap Orléans Laboratory, Orléans, France*
[11] *IHP Group, Angers, France*
[12] *Department of Translational Skin Cancer Research and Dermatology, University Hospital Essen, Essen, Germany*
[13] *German Cancer Consortium (DKTK), Partner Site Essen/Düsseldorf and German Cancer Research Center (DKFZ), Heidelberg, Germany*
[14] *Bioinformatics & Computational Biophysics, University Duisburg-Essen, Essen, Germany*
[15] *Department of Dermatology, Venereology and Allergology, University Hospital Würzburg, Würzburg, Germany*
[16] *Laboratoire de Biopathologie, CHRU de Nancy, Nancy, France*
[17] *INSERM U1256, Université de Lorraine, Nancy, France*
[18] *Department of Neuropathology, Institute of Pathology, Ruprecht-Karls-University, Heidelberg, Germany*
[19] *Clinical Cooperation Unit Neuropathology, German Cancer Research Center (DKFZ), and German Cancer Consortium (DKTK), Heidelberg, Germany*
[20] *Department of Dermatology, Université de Tours, Centre Hospitalier Universitaire de Tours, Tours, France*

**Correspondence to: T Kervarrec, Department of Pathology, Hôpital Trousseau, CHRU de Tours, 37044 TOURS Cedex 09, Tours, France.*
E-mail: thibaultkervarrec@yahoo.fr

†These authors contributed equally to this work.

Abstract

Merkel cell carcinoma (MCC) is an aggressive skin cancer frequently caused by genomic integration of the Merkel cell polyomavirus (MCPyV). MCPyV-negative cases often present as combined MCCs, which represent a distinctive subset of tumors characterized by association of an MCC with a second tumor component, mostly squamous cell carcinoma. Up to now, only exceptional cases of combined MCC with neuroblastic differentiation have been reported. Herein we describe two additional combined MCCs with neuroblastic differentiation and provide comprehensive morphologic, immunohistochemical, transcriptomic, genetic and epigenetic characterization of these tumors, which both arose in elderly men and appeared as an isolated inguinal adenopathy. Microscopic examination revealed biphasic tumors combining a poorly differentiated high-grade carcinoma with a poorly differentiated neuroblastic component lacking signs of proliferation. Immunohistochemical investigation revealed keratin 20 and MCPyV T antigen (TA) in the MCC parts, while neuroblastic differentiation was confirmed in the other component in both cases. A clonal relation of the two components can be deduced from 20 and 14 shared acquired point mutations detected by whole exome analysis in both combined tumors, respectively. Spatial transcriptomics demonstrated a lower expression of stem cell marker genes such as *SOX2* and *MCM2* in the neuroblastic component. Interestingly, although the neuroblastic part lacked TA expression, the same genomic MCPyV integration and the same large T-truncating mutations were observed in both tumor parts. Given that neuronal transdifferentiation upon TA repression has been reported for MCC cell lines, the most likely scenario for the two combined MCC/neuroblastic tumors is that neuroblastic transdifferentiation resulted from loss of TA expression in a subset of MCC cells. Indeed, DNA methylation profiling suggests an MCC-typical cellular origin for the combined MCC/neuroblastomas.

Keywords: Merkel cell carcinoma; neuroblastoma; polyomavirus

Received 2 January 2024; Revised 28 February 2024; Accepted 8 May 2024

No conflicts of interest were declared.

Introduction

Merkel cell carcinoma (MCC) is an aggressive skin cancer with an overall 5-year survival historically estimated at 40% [1,2]. At primary diagnosis, 26% of patients are diagnosed with regional disease and 8% with distant metastases [3]. Rarely, MCC located in a lymph node without detectable skin primary is diagnosed and is thought to represent metastasis from a subclinical or spontaneously regressed cutaneous tumor [4,5]. Besides neuroendocrine features, MCC cells exhibit some characteristics reminiscent of stem cells, which can contribute to the tumor's aggressive behavior. For example, MCC cells can express stem cell markers, such as SOX2, MCM2 and ABCB5 [6,7].

Recurrent genomic integration of the Merkel cell polyomavirus (MCPyV) in MCC was demonstrated in 2008 [8]. Indeed, the MCPyV genome is detected in about 80% of all MCC cases [8], and expression of the two viral oncoproteins, that is, small T (sT) and large T (LT), has been identified as the main oncogenic event in this subset of tumors [9,10]. Of note, integration-related gene alterations or mutations lead to expression of a truncated LT in MCPyV-positive MCC [11]. Sequestration and inactivation of RB1 by this truncated viral protein is required for tumor cell proliferation [10,12], while sT has been demonstrated to bear transforming abilities [9].

Behind their contribution to transformation and cell proliferation, the two T antigens (TAs) have been demonstrated to be main determinants of the Merkel-like phenotype of MCC tumor cells [13]. Notably, LT activates transcription of *SOX2* [6] and *ATOH1* [14], two genes encoding key transcription factors physiologically involved in Merkel cell differentiation [15]. Accordingly, knockdown of TA in MCC cell lines results not only in cell cycle arrest [10,12], but can also lead to neuronal differentiation under specific conditions [6]. Moreover, by interacting with MYCL and EP400, sT induces INSM1 as well as LSD1, an epigenetic modifier [16] regulating *ATOH1* expression. The significance of the latter mechanism is highlighted by the fact that chemical inhibition of LSD1 in MCC cell lines results not only in reduced cell growth, but also in expression of factors involved in neuronal differentiation [16,17].

The so-called combined MCCs found in association with a tumor of divergent differentiation [18,19] are a distinctive subset of MCCs accounting for about 10% of cases [20,21]. These combined MCCs are almost never related to MCPyV integration [19,22], mostly consist of an MCC with a squamous cell carcinoma component [20,22], while glandular, sarcomatoid or adnexal differentiation are also observed but rare [19,23,24]. MCCs combined with a tumor consisting of cells with an immature neuronal, a so-called 'neuroblastic' phenotype, have been reported so far only three times [19,25,26].

Here, we characterize two cases of combined MCPyV-positive MCCs presenting as lymph node metastases without skin primary tumors and harboring a neuroblastic component. Notably, we demonstrate a clonal relation between the two tumor components and demonstrate MCPyV integration in both components. Our analysis suggests that neuroblastic transdifferentiation in these cases results from loss of TA expression.

Materials and methods

Ethics

This study was approved by the local ethics committee (Tours, France, No. ID RCB2009-A01056-51). The analyses were performed with the written consent of the patients.

Immunohistochemistry

Immunohistochemical staining for Cytokeratins AE1/AE3, Cytokeratin 20, Chromogranin A, Synaptophysin, ISL1, CD56, Neurofilaments, SATB2, GFAP, PS100, PHOX2B, NeuN, Olig2, Ki67, SOX2, MCPyV TA/LT (AB3, CM2B4, 2T2 [27]) was performed using a BenchMark XT Platform (Tucson, AZ, USA). Antibodies and dilutions are listed in supplementary material, Table S1.

DNA isolation and MCPyV quantitative PCR

After microdissection of the two tumor components under a binocular magnifier, genomic DNA was isolated using the Maxwell 16 formalin-fixed and paraffin-embedded Plus LEV DNA purification kit (Promega, Madison, WI, USA). DNA from healthy tissue was obtained from peripheral blood mononuclear cells (PBMCs). MCPyV status determination by real-time PCR was performed as previously described [28].

Massive parallel sequencing

The DNAs derived from the neuroblastic tumor component and the PBMC were subjected to whole exome sequencing, while whole genome sequencing to facilitate detection of virus integration was performed with the DNA from the MCC components. See Supplementary materials and methods for details regarding sequencing, data analysis, somatic variant calling, copy number variation (CNV) analysis and detection of the viral integration sites [29–41].

Spatially resolved transcriptomics

Spatially resolved transcriptomics was performed on FFPE tissue of one of the combined tumors following the protocols for Visium CytAssist Spatial Gene Expression for FFPE (10× Genomics, Leiden, The Netherlands). A detailed description can be found in Supplementary materials and methods.

Analysis of DNA methylation

Genomic DNA was extracted from formalin fixed paraffin embedded tissues using Maxwell apparatus (Promega, Madison, WI, USA) with Maxwell 16 FFPE Plus LEV DNA Purification kits. Methylation profiling employed the MethylationEPIC BeadChip (Illumina, San Diego, CA, USA). 300 ng of DNA were processed according to the manufacturer's protocol as previously described [42]. Data were generated in the Department of Neuropathology of the University Hospital Heidelberg. Computational analyses were based on R version 4.6.1 (https://www.R-project.org). tSNE plot was generated on the 10,000 most variable CpG sites upon standard deviation, 3,000 iterations and 10 perplexities.

Results

Two combined tumors consisting of an MCPyV-positive MCC and a neuroblastic component

Analysis of the combined MCCs provides an exceptional opportunity to study the cellular origin as well as the molecular pathology of MCCs [22,23,43,44]. Therefore, two combined MCCs with neuroblastic components were extensively analyzed. The clinical and microscopic features of these two cases are presented in Table 1 and Figures 1 and 2. Both tumors arose as isolated inguinal adenopathy without detectable skin tumors or distant metastasis in a 75- and an 80-year-old man, respectively. Microscopic examination (Figure 1, supplementary material, Figure S1) revealed infiltration of the lymph nodes by a poorly differentiated high-grade carcinoma composed of monotonous tumor cells with high nucleocytoplasmic ratio, round nuclei and clear/fine chromatin associated with numerous mitotic figures and foci of necrosis, which are all features typically observed in classical MCCs.

In both tumor samples, in addition to the phenotypical classical MCC, a second tumor component—making up less than 5% of the tumor volume—with neuroblastic appearance was observed, and the transition from one phenotype to the other was abrupt. In the neuroblastic component of both cases, isolated tumor cells with small round nuclei harboring neurites were embedded in large amounts of eosinophilic fibrillar stroma evocative of neuropils. No pseudo-rosette formation was observed. In addition, in case 2, few large tumor cells with abundant cytoplasm, pale nuclei and prominent nucleoli similar to differentiated neuroblastic cells were detected, while ganglion cells, a cell population detected in mature neuroblastic tumors [45], were absent. Neither necrosis nor mitotic figures were detected in the neuroblastic components, indicating that the tumor was viable but not proliferative. Indeed, the proliferative index evaluated by Ki67 was higher than 70% in the classical MCC component and less than 1% in the neuroblastic component, confirming lack of proliferation in the latter.

Further immunohistochemical investigation (Table 1, Figure 2, supplementary material, Figure S2) revealed similar features in the classical MCC component of both cases, with co-expression of Keratin 20 and neuroendocrine markers. Importantly, the classical MCC component stained positive for MCPyV LT, while no expression of LT or Keratin 20 was observed in the neuroblastic components, which were further characterized by strong and diffuse expression of synaptophysin, neurofilament and CD56 in a fibrillar pattern. Interestingly, in addition to the advanced age of the patients, a further finding atypical for neuroblastic tumors was lack of the well established neuroblastic markers PHOX2B and GATA3 [46,47]. In contrast, GFAP, a marker for glial tumors [48,49], stained focally in the neuroblastic component, which also exhibited focal cytokeratin (AE1/AE3) staining. Further neuronal markers such as Olig2 and NeuN were, however, not detected, while S100 was detectable in some cells (supplementary material, Figure S3) as previously described for neuroblastic tumors [50].

The MCC and the neuroblastic components share common somatic alterations

Next, we addressed whether the two tumor components are genetically related or represent independent co-development of two tumors in the same anatomic location. The latter so-called collision tumors are rare but well documented [51]. To distinguish between the two possibilities, the MCC and the neuroblastic tumor components were micro-dissected for both patients, and DNA was isolated from the individual tumor components as well as from PBMCs as control. DNA from PBMCs and the neuroblastic tumor components was subjected to whole exome sequencing, while DNA from the MCC component was also analyzed by whole genome sequencing (WGS). These analyses (supplementary material, Tables S2 and S3) demonstrated 20 and 14 somatic DNA variants in case 1 and 2, respectively, common to both the MCC and

Table 1. Clinical, morphologic, immunohistochemical and genetic features of the two combined Merkel cell carcinomas (MCCs) with neuroblastic differentiation.

Clinical features	Case 1	Case 2
Age (years)	80	75
Sex	M	M
Immunosuppression	–	–
Tumor location	Inguinal lymph node No skin primary	Inguinal lymph node No skin primary
Extension work up	TEP	Thoracic scan Skin examination
Tumor size (mm)	33	33
Extension at time of diagnosis/AJCC stage	Located/IIIA	Located/IIIA
Follow-up		
Duration (months)	9	35
Event	–	Gastric metastasis and death

Microscopic features	Case 1		Case 2	
	MCC	Neuroblastic	MCC	Neuroblastic
Growth pattern				
Solid	++	–	++	–
Trabecular	+	–	+	–
Nested	–	+	–	+
Cytology				
Nuclear/cytoplasmic ratio	High	Medium	High	Medium
Nuclei (shape)	Round	Round	Round-oval	Round
Chromatin	Fine	Fine	Fine	Fine
Neurite	–	+	–	+
Mature neuroblast	–	–	–	+
Fibrillar stroma	–	+	–	+
Mitotic activity	32 mm^2	0	24 mm^2	0
Necrosis	+	–	+	–

Immunohistochemical features	Case 1		Case 2	
	MCC	Neuroblastic	MCC	Neuroblastic
CKAE1/AE3	++ dots	+ fibrillar	++ dots	+ fibrillar
CK20	++ dots	–	++ dots	–
Chromogranin A	+ dots	–	++	+
Synaptophysin	++	++ fibrillar	+	++ fibrillar
ISL1	++	+ weak	++	++
CD56	++	++ fibrillar	++	++
Neurofilament	+ dots	++ fibrillar	+ dots	++ fibrillar
SATB2	++	–	++	+
GFAP	–	+ fibrillar	–	+ fibrillar
S100	–	+ focal	–	+ focal
PHOX2B	–	–	–	–
NeuN	–	focal	–	–
Olig2	–	–	–	–
Ki67	80%	0	>70%	<2%
SOX2	++	–	++	–
AB3 (MCPyV LT)	++	–	++	–
CM2B4 (MCPyV LT)	++	–	++	–
2T2 (MCPyV TA)	++	–	NA	NA

Genetic features (common to two tumor parts)	Case 1	Case 2
Number of somatic variants	20	14
CNV alteration	Chr10 del	Chr10 del, 1p gain
MCPyV genomic integration	Chr11	Chr7

'–': lack, '+': presence, '++': intense and diffuse expression, Chr: chromosome, CNV: copy number variation, MCPyV: Merkel cell polyomavirus, NA: data not available.

neuroblastic components and not present in PBMCs from the same patient. These results indicate that the two tumor components are clonally related in both cases. Generally, higher allelic frequencies were observed in the MCC compared with the neuroblastic components, a finding that is likely due to a higher tumor cell content in the MCC component (Figure 1). Besides the shared variants, we also detected acquired sequence variants present only in one tumor component. In case 1, two variants (in *PTPN11* and *POM121L2*) were restricted to the MCC component, while in case 2, 7 and 11 variants were exclusively detected in the MCC and neuroblastic components, respectively. Based on these numbers, the similarity indices, which can be used to

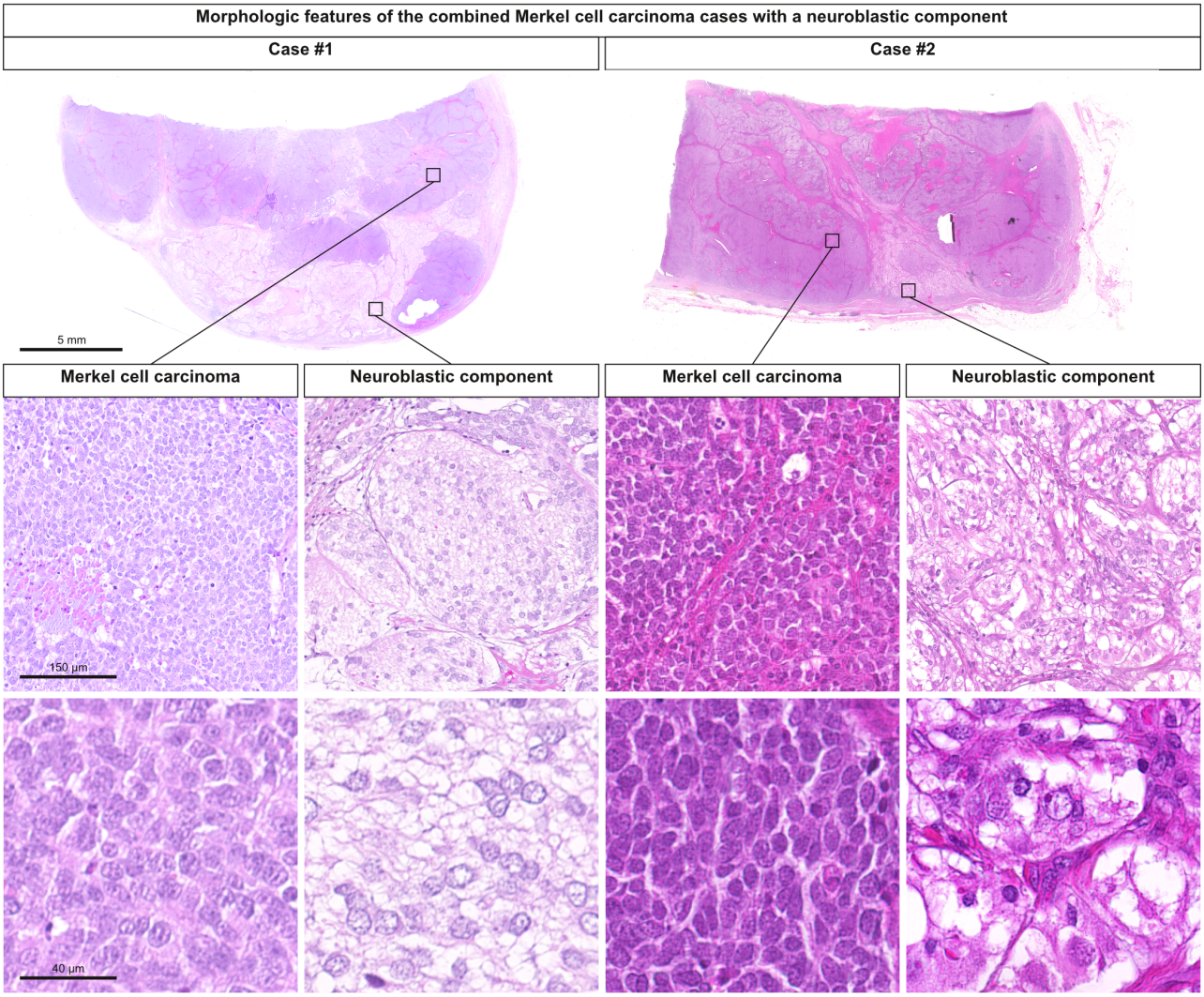

Figure 1. Morphologic features of the two combined Merkel cell carcinoma (MCC) cases with neuroblastic differentiation. Morphologic features of the cases (Hematein-phloxin saffron staining). Microscopic examination at low magnification revealed in both cases a biphasic neoplasm invading the lymph node (scale bar = 5 mm). Microscopic details of the cases (Hematein-phloxin saffron staining, scale bars = 150 and 40 µm). The MCC part (left panel) was predominant and consisted of solid sheets of poorly differentiated cells with high nucleocytoplasmic ratio, round to oval nuclei and fine chromatin. Numerous mitotic figures were observed. In contrast, the neuroblastic part (right panel) was characterized by non-proliferating tumor cells with small round nuclei harboring neurites and embedded in large amounts of eosinophilic fibrillar stroma. In case 2, few large tumor cells with abundant cytoplasm, pale nuclei and prominent nucleoli similar to differentiated neuroblastic cells were detected.

evaluate the clonal relation of two tumors [52], are calculated to be 0.91 and 0.42, respectively, indicating that 91% and 42% of the detected mutations are shared. In contrast, comparing mutations of the unrelated tumor parts yielded a similarity index of zero for all four possible comparisons. Given the small number of tumor DNAs investigated in our study, statistical evaluation of the similarity values as described [52] is not feasible. However, comparison with values obtained in similar projects [43,53] strongly suggests a clonal relationship of the two parts of the combined tumors described here.

Among the detected alterations, two variants with known pathogenic impact were identified in case 1: *ALK* p.(R1275Q) and *PTPN11* p.(Y63C), which have both been reported to be prevalent in neuroblastoma [54–56], but have also been detected rarely in MCCs [57]. The above-described mutations restricted to only one part of two clonally related tumor components can be explained by either being acquired following emergence of the two tumor components or by phenotypic changes having occurred in one tumor cell or a subpopulation of the original tumor specifically carrying and lacking these mutations, respectively.

CNV analysis (supplementary material, Figure S4) also demonstrated a degree of distance in tumor evolution between the two components of the combined tumors, since in case 1 the alterations in chromosome (chr) 1 are different, and an additional loss is observed in chr 7 of the MCC part in case 2. On the other hand, CNV analysis also supports a clonal link by demonstrating a chr 10 deletion common to the MCC and neuroblastic components in both cases, and a 1q gain in both components in case 2. Interestingly, alterations chr 10 deletion and chr 1 gain have been described as recurrent events in MCCs [57]. In

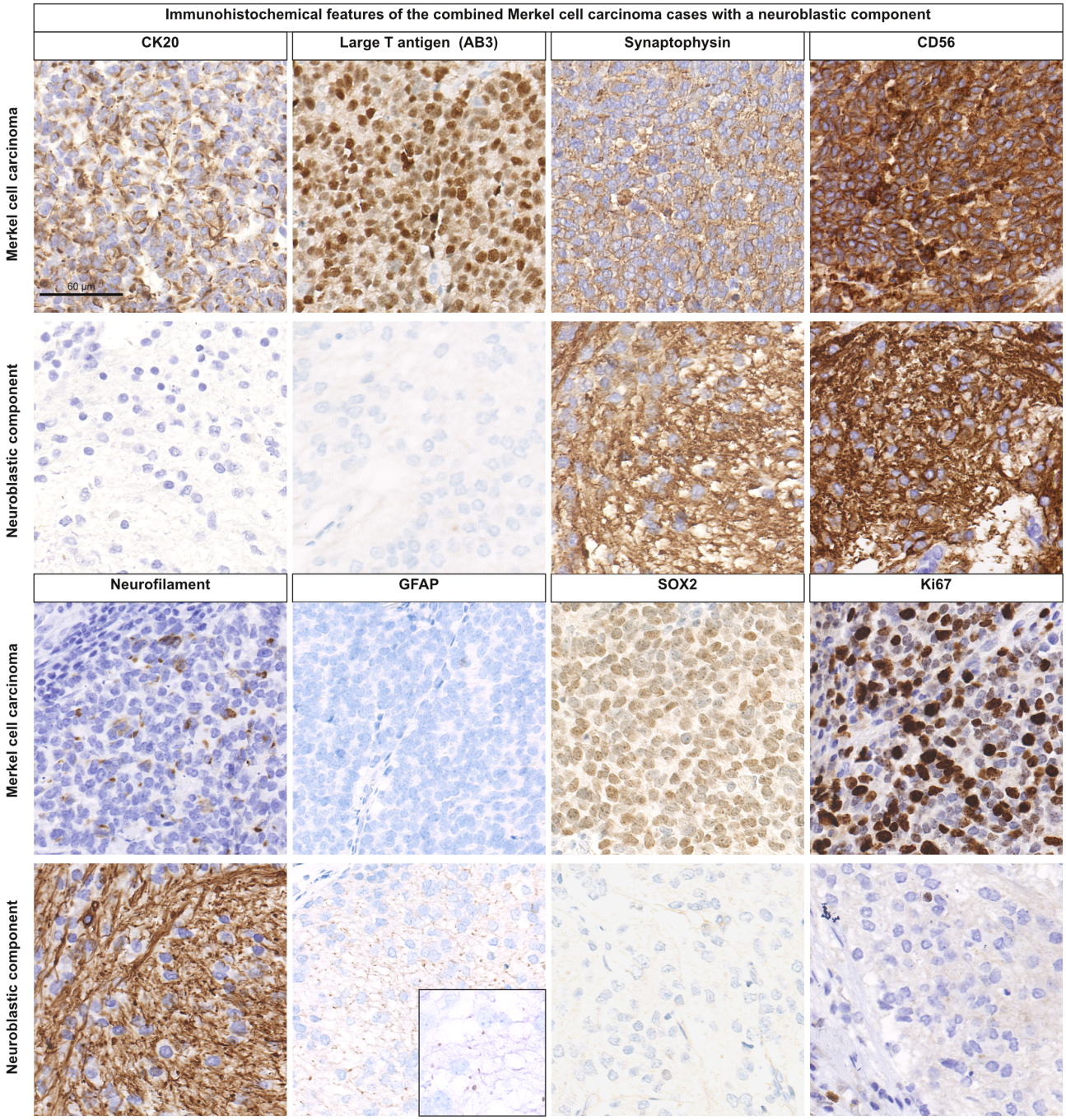

Figure 2. Immunohistochemical features of the combined Merkel cell carcinoma (MCC) with neuroblastic differentiation. Case 1 is depicted here and representative illustrations of immunohistochemical features of case 2 are available in supplementary material, Figure S2. Immunohistochemistry shows cytokeratin 20 (CK20), neuroendocrine markers (Synaptophysin, CD56) and large T antigen (clone Ab3) in the MCC part, while neurofilament (intense and diffuse) and GFAP expression with a fibrillar pattern are restricted to the neuroblastic component. Furthermore, high proliferation index (Ki67) and intense nuclear SOX2 positivity were detected in the MCC part but absent from the neuroblastic cells.

conclusion, although these sequencing data strongly support that the MCC and neuroblastic components of the combined tumors are clonally related in both cases, it cannot be concluded which evolved from the other.

Integration of MCPyV in the tumor cell genomes of MCC and neuroblastic components

To further understand the genotype of the two tumor components, we analyzed the presence of the MCPyV genome, since immunohistochemical analysis suggested MCPyV-related MCC oncogenesis. Indeed, using several different antibody clones (AB3, CM2B4 and 2 T2, Figure 2, Table 1), TA was detectable only in the MCC component of both cases. Therefore, we searched for viral sequences in the WGS data derived from the micro-dissected MCC components, detecting integration of MCPyV in chr 11 in case 1 and in chr 7 in case 2. While a 5'- and a 3'-prime integration site could be detected for case 1, we were only able to identify one of

the minimally two sites for case 2. Moreover, a LT-truncating mutation could be identified for both cases (p.Gln432* for case 1 and p.Ser293* for case 2). Therefore, both genetic hallmarks of MCPyV-positive MCC—MCPyV integration as well as a coding sequence for truncated LT—are present in the MCC component of the combined tumors.

In contrast to the MCC, no TA was detectable in the neuroblastic components, while PCR demonstrated similar MCPyV viral loads in the corresponding tumor components of both cases (data not shown). Based on the MCPyV integration sites in the MCC component inferred from WGS, we designed primers to amplify the respective integration sites. Strikingly, amplification of all known insertion sites as well as confirmation by Sanger sequencing was possible with DNA derived from the MCC and the neuroblastic component (Figure 3A). These findings indicate that the same MCPyV integration is common in both components, while TA expression is restricted to the MCC component in each of the combined tumors. Moreover, PCR followed by sequencing confirmed that the same LT-truncating mutations were present in both tumor components of both cases (Figure 3B,C). These results not only confirm the common origin of both tumor components, but also reveal that the two genetic key features of MCPyV-positive MCCs are present in both components of the combined MCCs. Nevertheless, the results still do not identify which component was derived from the other.

DNA methylation suggests an MCC-typical cell of origin for the combined MCC/neuroblastomas

To better understand the natural history of these combined tumors, we determined the DNA methylation profile of the two specimens in comparison to pure MCC (including 23 MCPyV-positive and 9 MCPyV-negative tumors) and neuroblastoma (including 10 adrenal and 23 peripheral cases). Methylation at CpG dinucleotides represents one of the major epigenetic mechanisms of

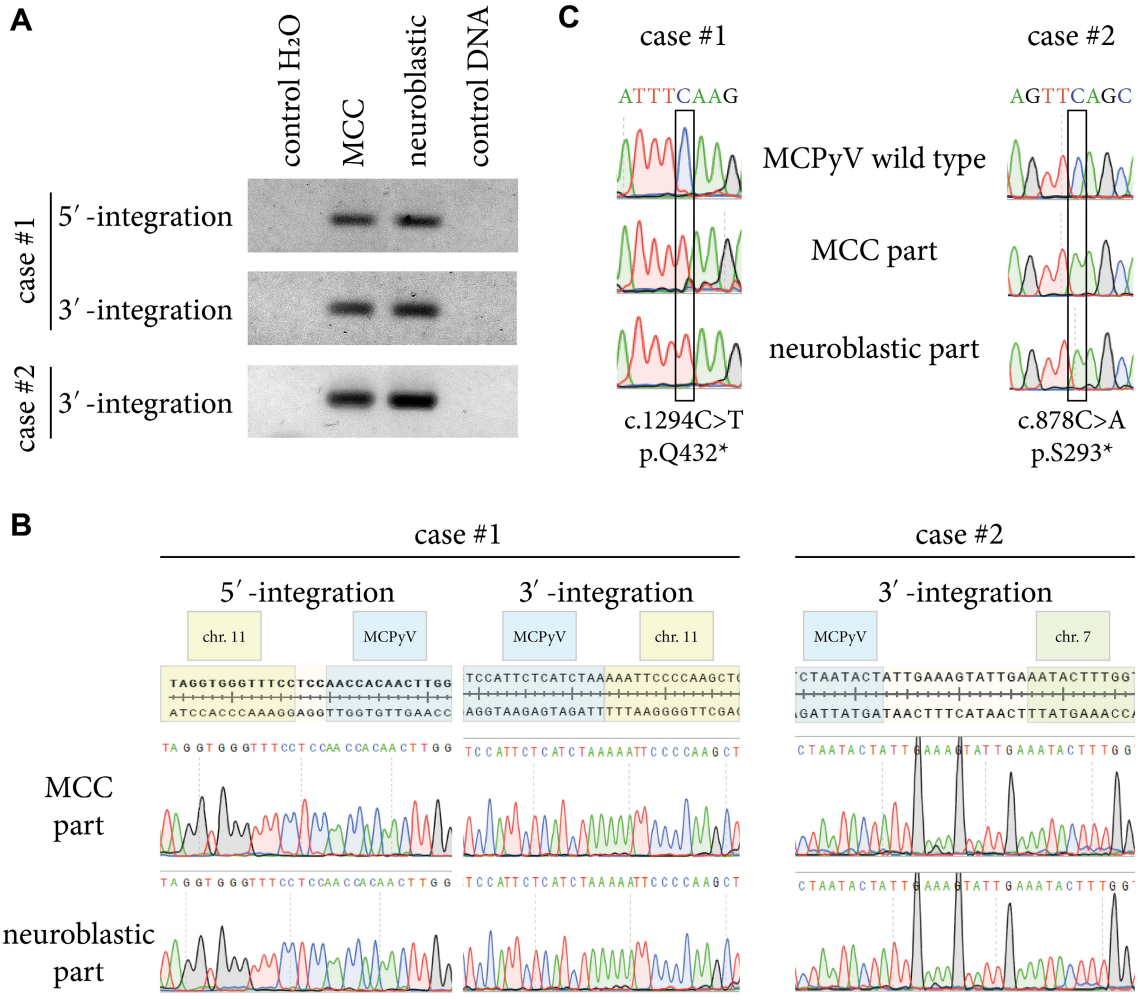

Figure 3. Demonstration of the same Merkel cell polyomavirus (MCPyV) integration and the same large T (LT)-truncating mutations in the corresponding Merkel cell carcinoma (MCC) and neuroblastic parts of the combined tumors. MCPyV integration in the tumor cell genomes as identified by exome sequencing was confirmed by PCR amplification of the junction sequences yielding (A) bands of the predicted size. (B) Sanger sequencing of the amplicons further confirmed equal virus integration in MCC and neuroblastic parts of both combined tumors. The chromosomal nucleotide positions of MCPyV integration are indicated. (C) PCR amplification followed by Sanger sequencing demonstrated the presence of the same LT-truncating mutations in MCC and neuroblastic parts. The alterations are indicated according to the standard mutation nomenclature in molecular diagnostics [58].

gene regulation [59], inherited during cell division, and the methylation pattern is regarded as a robust marker of cell identity [60]. With respect to cancer, the methylation pattern is considered a suitable method for classification and to identify a tumor's cell of origin [61,62]. Therefore, we subjected DNA derived from both MCC parts and one neuroblastic part of the two combined tumors to methylation analysis (sufficient material was not available from the neuroblastic part of case 2). Comparison of the methylation patterns with those of pure MCCs and neuroblastomas revealed that the combined tumors cluster with MCC, suggesting a similar origin and classifying the combined tumors as MCCs (Figure 4). In conclusion, the methylation pattern suggests a sequence of an MCC arising by integration of MCPyV in an MCC-characteristic cell of origin, followed by neuroblastic differentiation in a fraction of the preexisting MCC cells.

TA repression is associated with neuroblastic transdifferentiation

In cell culture experiments, neuronal differentiation has been reported to occur following knockdown of TA in MCC cell lines, and these changes are thought to be related to repression of SOX2 upon reduced TA activity [6]. Thus, we hypothesized that the neuroblastic component may have arisen from the MCPyV-positive MCC through TA repression. Indeed, immunohistochemistry of the two combined tumors revealed diffuse SOX2 in the MCC component, while this protein was lacking in the neuroblastic component (Figure 2). Prompted by this observation, we performed spatially resolved transcriptomics to examine gene expression patterns in a region-specific context of case 1 to investigate the transcriptomic differences between the two phenotypes (Figure 5A). After filtering out spots that were regarded as uncovered areas as the number of genes and unique molecular identifiers counts were low (supplementary material, Figure S5 cluster 6), 4,417 spots of the initial 4,918 spots were further analyzed. Dimensionality reduction resulted in a continuum of spots in UMAP space. Spatial clustering resulted in eight clusters, four located in the classical MCC region and two in the neuroblastic region, in addition to a fibroblast cluster and a carcinoma-associated fibroblast cluster (Figure 5B). Spatial clustering in enhanced resolution using BayesSpace, a fully Bayesian statistical method that uses the information from spatial neighborhoods, also demonstrated similar patterns, producing four classical neuroendocrine clusters and two neuronal clusters; the respective clustered spots were annotated by the predominant cellular content and re-projected to their original spatial context (Figure 5C). These results suggested that the classical MCC component displayed higher heterogeneity than the neuroblastic tumor part, which implies later occurrence of the latter. It was also possible to infer CNVs from the spatial transcriptomic data (supplementary material, Figure S6), which partially overlapped with the CNV deduced from sequencing (supplementary material, Figure S4). More importantly, however, the feasibility of this approach demonstrated the required purity with respect to tumor cell content of the spots selected for spatial transcriptomics and suggested higher genetic heterogeneity in the classical component than the neuroblastic part (supplementary material, Figure S7).

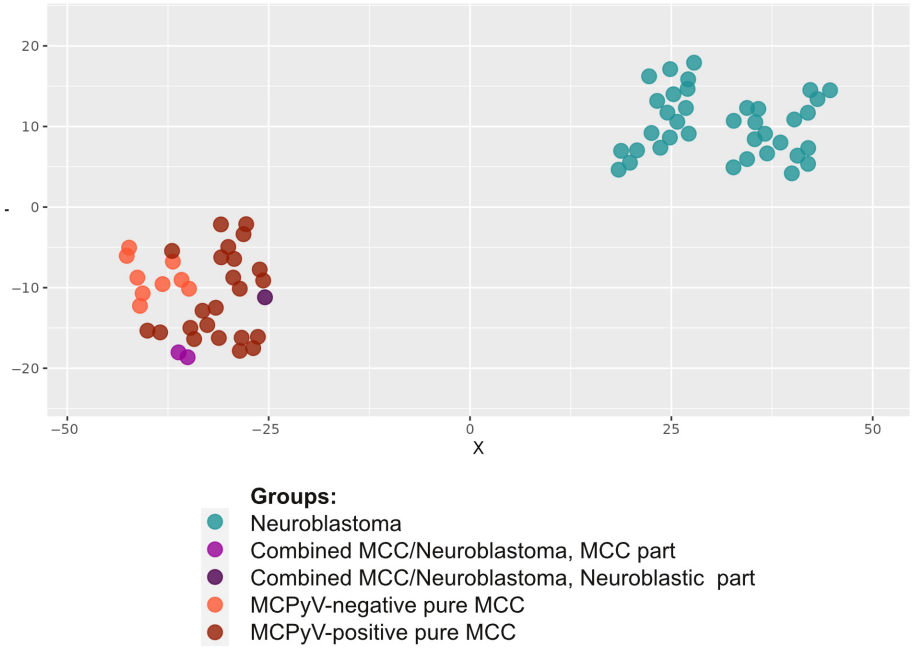

Figure 4. DNA methylation-based classification of the two combined tumors in comparison to Merkel cell carcinoma (MCC) and neuroblastoma. Methylation profiling with DNA extracted from the combined tumors (no material was left for the neuroblastic part of case 2) as well as 32 pure MCCs and 33 pure neuroblastomas. Depicted is unsupervised clustering using t-SNE dimensionality reduction. Neuroblastoma: shades of blue; MCC: shades of red; combined MCC/neuroblastoma 1 and 2: shades of violet.

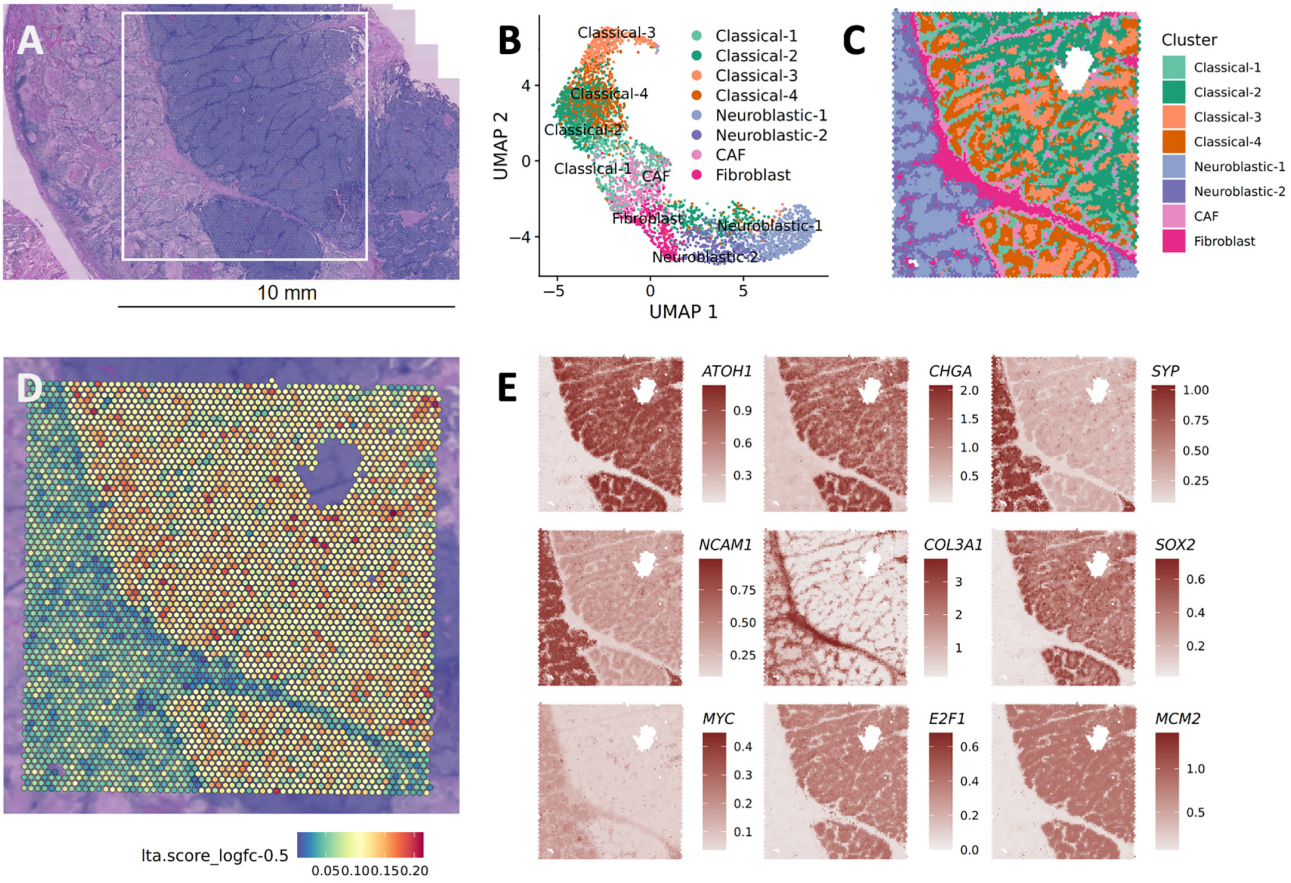

Figure 5. Spatially resolved RNA-sequencing analysis of one combined Merkel cell carcinoma (MCC)/neuroblastoma. (A) H&E visualizing classical MCC (dark purple, right) and neuroblastic tumor cells (pale pink, left). The white frame represents the area selected for spatial RNA sequencing. (B) UMAP representation of spatial neighbor network unsupervised clustering of the filtered spots. Spatial clusters were renamed based on histological features and gene marker expressions: four classical MCC and two neuroblastic clusters as well as fibroblasts and carcinoma associated fibroblasts (CAFs). (C) Spatial representation of the spots grouped into eight spatial clusters in enhanced resolution. (D) Spatial visualization of AUCell scores of T antigen (TA)-associated gene panel inferred by differential expression analysis of TA knockdown experiment in CVG-1 cell line, where only genes with log2 fold change >0.5 were considered. (E) Inferred gene expressions of tumor markers in enhanced spot resolution. *ATOH1* and *CHGA*: neuroendocrine markers; *SYP* and *NCAM1*: neuroblast markers; *COL1A1*: fibroblast; *MCM* and *E2F* genes: large T antigen associated markers.

Since FFPE Visium does not contain probes for viral genes, we applied an LT-associated gene expression score derived from publicly available single-cell RNA sequencing data [6], demonstrating a markedly lower score in neuroblastic compared with classical MCCs [6] (Figure 5D); notably, this score was very low in spots characterized by mainly fibroblasts.

When inspecting specific gene expression, we observed increased neuroendocrine lineage markers *ATOH-1* and *CHGA* (chromogranin A) in the classical MCC, whereas *SYP* (synaptophysin) and *NCAM1* (neural cell adhesion molecule 1) were higher in the neuroblastic component (Figure 5E), confirming the immunohistochemical studies (Figure 2). Similarly, in line with the abundance of mitotic figures and high Ki67 (Figures 1, 2), genes associated with cell proliferation were higher in the MCC component (data not shown). Moreover, *SOX2* was reduced in the neuroblastic component of the combined tumor, consistent with previous observations on SOX2-dependent conversion of undifferentiated MCC cells into neuronal phenotypes [6]. In cell culture experiments, reduced stemness and enhanced neural phenotypes observed upon TA knockdown in MCC cells was associated with reduced stemness regulators E2F1 and MCM2 [6,63,64]. Similarly, we also noticed downregulation of *E2F* and *MCM* mRNAs in the neuroblastic component of the combined tumor (Figure 5E). Moreover, *MYCN*, a member of the MYC family that is highly expressed during early neurogenesis and plays a critical role in survival of neural progenitor cells [65], was upregulated in the neuroblastic component compared with the classical MCC or fibroblast spots (Figure 5E). In conclusion, reduced heterogeneity as well as lack of proliferation in the neuroblastic component and the observed expression patterns analogous to TA knockdown in MCC cell lines *in vitro* further support the view that neuroblastic differentiation occurred in a fraction of a preexisting MCCs upon loss of TA expression.

Discussion

Combined MCCs account for approximately 10% of all MCCs and their development is likely to reflect several

different pathophysiologic mechanisms. However, most combined cases are MCCs associated with a squamous cell carcinoma or a respective precursor lesion [19,20] and the MCC component of these combined tumors is generally MCPyV negative [18,19]. Individual genetic investigation of the two tumor components in such cases revealed a generally common genetic background, demonstrating that the MCC component usually derives from the squamous cell carcinoma component, demonstrating the epithelial origin of virus-negative MCCs [22,43,44]. In these tumors, the MCC component might even experience sarcomatoid transformation [24], explaining the existence of rare combined tumors with both squamous and sarcomatous differentiation [19]. In contrast, MCPyV-positive combined MCCs are very rare and seem not to occur in combination with SCCs, but have been described in association with benign adnexal tumors [21,23,66–68]. Applying WGS to two trichoblastoma/MCC combined cases, we recently reported that a MCPyV-positive MCC developed upon integration of MCPyV into the genome of a trichoblastoma cell [23,68].

Neuroblastic tumors arise from adrenal medulla and paraganglia and subdivide into three categories according to their level of differentiation: neuroblastoma, ganglioneuroblastoma and ganglioneuroma [69]. MCC with neuroblastic differentiation is very uncommon and only a few cases have been reported [19,20,25,26], and in our opinion constitute a heterogeneous subgroup due to the lack of consensual criteria to define 'neuroblastic' differentiation. Homer-Wright Rosette formations [19,20,70] can be observed in MCPyV-negative MCCs [19,70] and have been regarded as a sign of 'neuroblastic differentiation'. However, these morphologic changes were not associated with documented modifications in protein/gene expression by immunohistochemistry or mRNA analysis. Combined tumors with an MCC and a neuroblastic or ganglioneuroblastic component seem to be even less frequent, with up to now only two case reports, which both lacked molecular characterization [25,26].

In the present work, we demonstrated that MCPyV-positive MCCs can be found in association with a neuroblastic component. By analyzing shared somatic pathogenic variants, we were able to identify a clonal link between these two tumor components. Finally, demonstration of MCPyV integration in both MCC and neuroblastic components and transcriptomic and epigenomic analysis suggest that the neuroblastic component arose from the MCC through a transdifferentiation process related to loss of TA expression. In line with this conclusion, cells from the neuroblastic component lack any sign of proliferation. Notably, MCPyV-positive MCC cells generally require TA expression for their growth [12]. Unfortunately, the limited experimental options studying archived tumor material did not allow us to determine the underlying mechanism for this loss of TA expression. In this context, future studies are required to determine the molecular event leading to TA repression, and such findings have potential impact for the development of innovative MCC therapy.

Several *in vitro* experiments including our own support the view that MCPyV-positive MCC cells can undergo neuronal transdifferentiation [6,14,17]. In this respect, repression of TA through RNA interference in MCC cell lines results in cell cycle arrest due to regained RB1 activity [10,12]. Accordingly, in contrast to the MCC component, no mitotic figures and low proliferative index (<1%) were observed in the neuroblastic component of the combined tumors described here (Figure 2). Moreover, TA repression and subsequent RB1 release results in loss of SOX2 and ATOH1, two key factors driving Merkel cell differentiation [15], providing an explanation for loss of the Merkel cell phenotype upon loss of TA expression. Importantly, under specific culture conditions (e.g. co-culture with keratinocytes), TA knockdown in MCPyV-positive MCC cell lines results in formation of cytoplasmic projections similar to neurites, repression of epithelial gene expression, and transcription of neuronal markers such as neurofilaments [6]. Moreover, similar findings were observed upon SOX2 knockdown, suggesting that loss of TA induces neuronal differentiation through SOX2 inhibition. Accordingly, in our cases, while diffuse SOX2 was observed in the MCC component, absence of TA in the neuroblastic component was associated with lack of SOX2 [6]. While Harold *et al.* used this conversion from an MCC to a neuronal phenotype as an argument in favor of a neuronal origin of MCC [6], there is no evidence that TA expression in a neuronal cell is able to induce MCPyV-positive MCC formation. In contrast, TA expression in epithelial progenitor cells has been shown to be associated with MCC formation in humans and a mouse model [23,71,72], strongly supporting the view that virus-positive MCC and virus-negative MCC arise from epithelial cells [62].

In conclusion, we describe two cases of combined tumors with MCPyV-positive MCC and neuroblastic components, and demonstrate a clonal link between these two tumor components. Moreover, we provide data suggesting that part of the preexisting MCC undergoes neuroblastic transdifferentiation and cell cycle arrest upon loss of TA expression.

Acknowledgements

The authors thank Dr Christopher B. Buck for providing the 2T2 antibody. The authors thank Fondation ARC pour la recherche contre le cancer, Interdisziplinäres Zentrum für Klinische Forschung Würzburg (IZKF B-343) the German Research Foundation (SCHR 1178/3-2), the Ligue Nationale Contre le Cancer, Comités 16, 18, 28, HUGO Grant. German Cancer Consortium (DKTK), ED003, Illumina Grant.

Author contributions statement

TK, DS and RH performed study concept and design; TK, SA, JCB, AT, SeG, MS, AVD, DS and RH

performed development of methodology and writing, review and revision of the paper; SuG, EC, KB, RA, NM, RA, YL, JK, SK, NS, HS, AVD, AL, KCL and EMS provided acquisition, analysis and interpretation of data, and statistical analysis. All authors read and approved the final paper.

Data availability statement

The data set will be available in the European Genome Phenome Archive.

References

1. Becker JC, Stang A, DeCaprio JA, *et al*. Merkel cell carcinoma. *Nat Rev Dis Primer* 2017; **3:** 17077.
2. Becker JC, Stang A, Hausen AZ, *et al*. Epidemiology, biology and therapy of Merkel cell carcinoma: conclusions from the EU project IMMOMEC. *Cancer Immunol Immunother* 2018; **67:** 341–351.
3. Harms KL, Healy MA, Nghiem P, *et al*. Analysis of prognostic factors from 9387 Merkel cell carcinoma cases forms the basis for the new 8th edition AJCC staging system. *Ann Surg Oncol* 2016; **23:** 3564–3571.
4. Lemos BD, Storer BE, Iyer JG, *et al*. Pathologic nodal evaluation improves prognostic accuracy in Merkel cell carcinoma: analysis of 5823 cases as the basis of the first consensus staging system. *J Am Acad Dermatol* 2010; **63:** 751–761.
5. Kervarrec T, Zaragoza J, Gaboriaud P, *et al*. Differentiating Merkel cell carcinoma of lymph nodes without a detectable primary skin tumor from other metastatic neuroendocrine carcinomas: the ELECTHIP criteria. *J Am Acad Dermatol* 2018; **78:** 964–972.e3.
6. Harold A, Amako Y, Hachisuka J, *et al*. Conversion of Sox2-dependent Merkel cell carcinoma to a differentiated neuron-like phenotype by T antigen inhibition. *Proc Natl Acad Sci U S A* 2019; **116:** 20104–20114.
7. Kleffel S, Lee N, Lezcano C, *et al*. ABCB5-targeted chemoresistance reversal inhibits Merkel cell carcinoma growth. *J Invest Dermatol* 2016; **136:** 838–846.
8. Feng H, Shuda M, Chang Y, *et al*. Clonal integration of a polyomavirus in human Merkel cell carcinoma. *Science* 2008; **319:** 1096–1100.
9. Shuda M, Guastafierro A, Geng X, *et al*. Merkel cell polyomavirus small T antigen induces cancer and embryonic Merkel cell proliferation in a transgenic mouse model. *PLoS One* 2015; **10:** e0142329.
10. Houben R, Shuda M, Weinkam R, *et al*. Merkel cell polyomavirus-infected Merkel cell carcinoma cells require expression of viral T antigens. *J Virol* 2010; **84:** 7064–7072.
11. Shuda M, Feng H, Kwun HJ, *et al*. T antigen mutations are a human tumor-specific signature for Merkel cell polyomavirus. *Proc Natl Acad Sci U S A* 2008; **105:** 16272–16277.
12. Houben R, Adam C, Baeurle A, *et al*. An intact retinoblastoma protein-binding site in Merkel cell polyomavirus large T antigen is required for promoting growth of Merkel cell carcinoma cells. *Int J Cancer* 2012; **130:** 847–856.
13. Kervarrec T, Samimi M, Guyétant S, *et al*. Histogenesis of Merkel cell carcinoma: a comprehensive review. *Front Oncol* 2019; **9:** 451.
14. Fan K, Gravemeyer J, Ritter C, *et al*. MCPyV large T antigen-induced atonal homolog 1 is a lineage-dependency oncogene in Merkel cell carcinoma. *J Invest Dermatol* 2020; **140:** 56–65.e3.
15. Perdigoto CN, Bardot ES, Valdes VJ, *et al*. Embryonic maturation of epidermal Merkel cells is controlled by a redundant transcription factor network. *Development* 2014; **141:** 4690–4696.
16. Park DE, Cheng J, McGrath JP, *et al*. Merkel cell polyomavirus activates LSD1-mediated blockade of non-canonical BAF to regulate transformation and tumorigenesis. *Nat Cell Biol* 2020; **22:** 603–615.
17. Leiendecker L, Jung PS, Krecioch I, *et al*. LSD1 inhibition induces differentiation and cell death in Merkel cell carcinoma. *EMBO Mol Med* 2020; **12:** e12525.
18. Pulitzer MP, Brannon AR, Berger MF, *et al*. Cutaneous squamous and neuroendocrine carcinoma: genetically and immunohistochemically different from Merkel cell carcinoma. *Mod Pathol* 2015; **28:** 1023–1032.
19. Martin B, Poblet E, Rios JJ, *et al*. Merkel cell carcinoma with divergent differentiation: histopathological and immunohistochemical study of 15 cases with PCR analysis for Merkel cell polyomavirus. *Histopathology* 2013; **62:** 711–722.
20. Walsh NM. Primary neuroendocrine (Merkel cell) carcinoma of the skin: morphologic diversity and implications thereof. *Hum Pathol* 2001; **32:** 680–689.
21. Ogawa T, Donizy P, Wu C-L, *et al*. Morphologic diversity of Merkel cell carcinoma. *Am J Dermatopathol* 2020; **42:** 629–640.
22. Kervarrec T, Appenzeller S, Samimi M, *et al*. Merkel cell polyomavirus-negative Merkel cell carcinoma originating from in situ squamous cell carcinoma: a keratinocytic tumor with neuroendocrine differentiation. *J Invest Dermatol* 2022; **142:** 516–527.
23. Kervarrec T, Aljundi M, Appenzeller S, *et al*. Polyomavirus-positive Merkel cell carcinoma derived from a trichoblastoma suggests an epithelial origin of this Merkel cell carcinoma. *J Invest Dermatol* 2020; **140:** 976–985.
24. Barbieux S, Tallet A, Collin C, *et al*. Genetic evidence of a sarcomatoid transformation in Merkel cell carcinoma. *J Eur Acad Dermatol Venereol* 2023; **37:** e45–e48.
25. Vanchinathan V, Marinelli EC, Kartha RV, *et al*. A malignant cutaneous neuroendocrine tumor with features of Merkel cell carcinoma and differentiating neuroblastoma. *Am J Dermatopathol* 2009; **31:** 193–196.
26. Lach B, Joshi SS, Murty N, *et al*. Transformation of Merkel cell carcinoma to ganglioneuroblastoma in intracranial metastasis. *Hum Pathol* 2014; **45:** 1978–1981.
27. Wang X, Li J, Schowalter RM, *et al*. Bromodomain protein Brd4 plays a key role in Merkel cell polyomavirus DNA replication. *PLoS Pathog* 2012; **8:** e1003021.
28. Kervarrec T, Tallet A, Miquelestorena-Standley E, *et al*. Diagnostic accuracy of a panel of immunohistochemical and molecular markers to distinguish Merkel cell carcinoma from other neuroendocrine carcinomas. *Mod Pathol* 2019; **32:** 499–510.
29. Jiang H, Lei R, Ding S-W, *et al*. Skewer: a fast and accurate adapter trimmer for next-generation sequencing paired-end reads. *BMC Bioinformatics* 2014; **15:** 182.
30. Andrews S. FastQC: A Quality Control Tool for High Throughput Sequence Data (v0.11.9). 2010. [Accessed 1 March 2023]. Available from: http://www.bioinformatics.babraham.ac.uk/projects/fastqc/.
31. Krueger F. TrimGalore (v0.6.4). 2023. [Accessed 19 November 2019]. Available from: http://www.bioinformatics.babraham.ac.uk/projects/trim_galore/.
32. Picard-slim. [Accessed 1 May 2022]. Available form: https://anaconda.org/bioconda/picard-slim (v.2.25.0).
33. Kechin A, Boyarskikh U, Kel A, *et al*. cutPrimers: a new tool for accurate cutting of primers from reads of targeted next generation sequencing. *J Comput Biol* 2017; **24:** 1138–1143.
34. Li H, Handsaker B, Wysoker A, *et al*. The sequence alignment/map format and SAMtools. *Bioinformatics* 2009; **25:** 2078–2079.
35. Li H, Durbin R. Fast and accurate short read alignment with burrows-wheeler transform. *Bioinformatics* 2009; **25:** 1754–1760.
36. McKenna A, Hanna M, Banks E, *et al*. The genome analysis toolkit: a mapreduce framework for analyzing next-generation DNA sequencing data. *Genome Res* 2010; **20:** 1297–1303.

37. Koboldt DC, Zhang Q, Larson DE, *et al*. VarScan 2: somatic mutation and copy number alteration discovery in cancer by exome sequencing. *Genome Res* 2012; **22:** 568–576.
38. Wang K, Li M, Hakonarson H. ANNOVAR: functional annotation of genetic variants from high-throughput sequencing data. *Nucleic Acids Res* 2010; **38:** e164.
39. Thorvaldsdóttir H, Robinson JT, Mesirov JP. Integrative genomics viewer (IGV): high-performance genomics data visualization and exploration. *Brief Bioinform* 2013; **14:** 178–192.
40. Liang Y, Qiu K, Liao B, *et al*. Seeksv: an accurate tool for somatic structural variation and virus integration detection. *Bioinformatics* 2017; **33:** 184–191.
41. bcl2fastq. [Accessed 30 August 2017]. Available from: https://support.illumina.com/sequencing/sequencing_software/bcl2fastq-conversion-software.html (v2.19).
42. Capper D, Jones DTW, Sill M, *et al*. DNA methylation-based classification of central nervous system tumours. *Nature* 2018; **555:** 469–474.
43. Harms PW, Verhaegen ME, Hu K, *et al*. Genomic evidence suggests that cutaneous neuroendocrine carcinomas can arise from squamous dysplastic precursors. *Mod Pathol* 2022; **35:** 506–514.
44. DeCoste RC, Walsh NM, Gaston D, *et al*. RB1-deficient squamous cell carcinoma: the proposed source of combined Merkel cell carcinoma. *Mod Pathol* 2022; **35:** 1829–1836.
45. Shimada H, Jarzembowski JA, Tonini GP, *et al*. Neuroblastoma. In *WHO Classification of Tumours Editorial Board. Endocrine and Neuroendocrine Tumours* (Vol. **10**, 5th edn). International Agency for Research on Cancer: Lyon, France, 2022 (WHO classification of tumours series).
46. Bielle F, Fréneaux P, Jeanne-Pasquier C, *et al*. PHOX2B immunolabeling: a novel tool for the diagnosis of undifferentiated neuroblastomas among childhood small round blue-cell tumors. *Am J Surg Pathol* 2012; **36:** 1141–1149.
47. Mohanty SK, Diwaker P, Mishra SK, *et al*. Diagnostic utility of GATA3 and ISL1 in differentiating neuroblastoma from other pediatric malignant small round blue cell tumors. *Int J Surg Pathol* 2024; **32:** 294–303.
48. Ikota H, Kinjo S, Yokoo H, *et al*. Systematic immunohistochemical profiling of 378 brain tumors with 37 antibodies using tissue microarray technology. *Acta Neuropathol* 2006; **111:** 475–482.
49. Kimura T, Budka H, Soler-Federsppiel S. An immunocytochemical comparison of the glia-associated proteins glial fibrillary acidic protein (GFAP) and S-100 protein (S100P) in human brain tumors. *Clin Neuropathol* 1986; **5:** 21–27.
50. Shimada H, Aoyama C, Chiba T, *et al*. Prognostic subgroups for undifferentiated neuroblastoma: immunohistochemical study with anti-S-100 protein antibody. *Hum Pathol* 1985; **16:** 471–476.
51. Bulte CA, Hoegler KM, Khachemoune A. Collision tumors: a review of their types, pathogenesis, and diagnostic challenges. *Dermatol Ther* 2020; **33:** e14236.
52. Burres SA. Facial biomechanics: the standards of normal. *Laryngoscope* 1985; **95:** 708–714.
53. Lazo de la Vega L, Bick N, Hu K, *et al*. Invasive squamous cell carcinomas and precursor lesions on UV-exposed epithelia demonstrate concordant genomic complexity in driver genes. *Mod Pathol* 2020; **33:** 2280–2294.
54. Pugh TJ, Morozova O, Attiyeh EF, *et al*. The genetic landscape of high-risk neuroblastoma. *Nat Genet* 2013; **45:** 279–284.
55. Mossé YP, Laudenslager M, Longo L, *et al*. Identification of ALK as a major familial neuroblastoma predisposition gene. *Nature* 2008; **455:** 930–935.
56. Bentires-Alj M, Paez JG, David FS, *et al*. Activating mutations of the noonan syndrome-associated SHP2/PTPN11 gene in human solid tumors and adult acute myelogenous leukemia. *Cancer Res* 2004; **64:** 8816–8820.
57. Starrett GJ, Thakuria M, Chen T, *et al*. Clinical and molecular characterization of virus-positive and virus-negative Merkel cell carcinoma. *Genome Med* 2020; **12:** 30.
58. Ogino S, Gulley ML, den Dunnen JT, *et al*. Standard mutation nomenclature in molecular diagnostics: practical and educational challenges. *J Mol Diagn* 2007; **9:** 1–6.
59. Zhang G, Pradhan S. Mammalian epigenetic mechanisms. *IUBMB Life* 2014; **66:** 240–256.
60. Loyfer N, Magenheim J, Peretz A, *et al*. A DNA methylation atlas of normal human cell types. *Nature* 2023; **613:** 355–364.
61. Hoadley KA, Yau C, Hinoue T, *et al*. Cell-of-origin patterns dominate the molecular classification of 10,000 tumors from 33 types of cancer. *Cell* 2018; **173:** 291–304.e6.
62. Gravemeyer J, Spassova I, Verhaegen ME, *et al*. DNA-methylation patterns imply a common cellular origin of virus- and UV-associated Merkel cell carcinoma. *Oncogene* 2022; **41:** 37–45.
63. Fu Y, Hu C, Du P, *et al*. E2F1 maintains gastric cancer stemness properties by regulating stemness-associated genes. *J Oncol* 2021; **2021:** 6611327.
64. Zhou X, Luo J, Xie H, *et al*. MCM2 promotes the stemness and sorafenib resistance of hepatocellular carcinoma cells via hippo signaling. *Cell Death Discov* 2022; **8:** 418.
65. Chen J, Guan Z. Function of oncogene Mycn in adult neurogenesis and oligodendrogenesis. *Mol Neurobiol* 2022; **59:** 77–92.
66. Battistella M, Durand L, Jouary T, *et al*. Primary cutaneous neuroendocrine carcinoma within a cystic trichoblastoma: a nonfortuitous association? *Am J Dermatopathol* 2011; **33:** 383–387.
67. Peralta I, Dacey EB, King R. Merkel cell carcinoma in situ arising in association with an infundibular cyst with unusual reticulated infundibulocystic proliferation. *Am J Dermatopathol* 2023; **45:** e58–e60.
68. Kervarrec T, Appenzeller S, Tallet A, *et al*. Detection of wildtype Merkel cell polyomavirus genomic sequence and VP1 transcription in a subset of Merkel cell carcinoma. *Histopathology* 2024; **84:** 356–368.
69. Choi JH, Ro JY. Mediastinal neuroblastoma, ganglioneuroblastoma, and ganglioneuroma: pathology review and diagnostic approach. *Semin Diagn Pathol* 2022; **39:** 120–130.
70. Kervarrec T, Tallet A, Miquelestorena-Standley E, *et al*. Morphologic and immunophenotypical features distinguishing Merkel cell polyomavirus-positive and negative Merkel cell carcinoma. *Mod Pathol* 2019; **32:** 1605–1616.
71. Verhaegen ME, Harms PW, Van Goor JJ, *et al*. Direct cellular reprogramming enables development of viral T antigen-driven Merkel cell carcinoma in mice. *J Clin Invest* 2022; **132:** e152069.
72. Weber M, Nguyen MB, Li MY, *et al*. Merkel cell polyomavirus T antigen-mediated reprogramming in adult Merkel cell progenitors. *J Invest Dermatol* 2023; **143:** 2163–2176.e6.

SUPPLEMENTARY MATERIAL ONLINE

Supplementary materials and methods

Figure S1. Microscopic feature of the neuroblastic component in combined tumors

Figure S2. Immunohistochemical features of case 2

Figure S3. S100 expression in combined tumors

Figure S4. Copy number variation analysis of both neuroblastic and Merkel cell carcinoma components of the two cases

Figure S5. Preliminary graph-based clustering of the spatial RNA sequencing data produced eight clusters among 4,918 spots

Figure S6. Copy number variation analysis generated by spatial transcriptomic analysis

Figure S7. Hierarchical clustering of the classical and neuroblastic Merkel cell carcinoma (MCC) spots based on inferred copy number variation (CNV) profiles suggests that neuroblastic MCC is more homogeneous than classical MCC, indicating neuroblastic MCC originates from classical MCC

Table S1. Antibodies used for immunohistochemistry

Table S2. Description of the somatic mutations detected by whole exome sequencing in the neuroblastic (NB) and the Merkel cell carcinoma (MCC) part of the combined tumor (case 1)

Table S3. Description of the somatic mutations detected by whole exome sequencing in the neuroblastic (NB) and the Merkel cell carcinoma (MCC) part of the combined tumor (case 2)